Supplementary information

Extended Data Vedio 1 *Ex vivo* two-photon imaging of skull BM at 7 days after IC injection of AF488-OVA-labeled yCSF. Intravenous (IV) injection of CD31 labeled vasculature. Scale bar, 147.3 μm.

Extended Data Table 1 Primers used for genotyping.

Gene	**Primer sequence (5'-3')**
tdTomoto P1	AAGGGAGCTGCAGTGGAGTA
tdTomoto P2	CCGAAAATCTGTGGGAAGTC
tdTomoto P3	GGCATTAAAGCAGCGTATCC
tdTomoto P4	CTGTTCCTGTACGGCATGG
Pdgfra-CreERT2 P1	TGCTCAAAACCATCTTCTCCTTC
Pdgfra-CreERT2 P2	TGGGACATGCTTCCACTGAC
Pdgfra-CreERT2 P3	CGCGCGCCTGAAGATATAGA
Mmp25 flox P1	ACCCGCAACTGGGATCACACA
Mmp25 flox P2	ACACAATCATGGCCCCTATCCC
Mmp25 flox P3	ACGCCCAGATGCAGAGTCTTG
Mmp25 flox P4	GGGACCAGATTTGTTCTGTCCC

Extended Data Table 2 Primers used for quantitative qPCR analysis.

Gene	Primer sequence (5'-3')
MMP25 (human)	F: CATTATGAGGCCCTTCTACCAGG
	R: CGCCTTCCCATAGAGTTGCTG
RUNX2 (human)	F: TCTTAGAACAAATTCTGCCCTTT
	R: TGCTTTGGTCTTGAAATCACA
IL6 (human)	F: CGCAACAACTCATCTCATTCTGCG
	R: CATGCTACATTTGCCGAAGAGC
PPARγ (human)	F: CGAGACCAACAGCTTCTCCTTCTCG
	R: TTTCAGAAATGCCTTGCAGTGG
LPL (human)	F: CGGATTAACATTGGAGAAGCTATCCG
	R: AGCTGGTCCACATCTCCAAGTC
P16 (human)	F: GATCCAGGTGGGTAGAAGGTC
	R: CCCCTGCAAACTTCGTCCT
P21 (human)	F: CGATGGAACTTCGACTTTGTCA
	R: GCACAAGGGTACAAGACAGTG
IL1B (human)	F: TTCGACACATGGGATAACGAGG
	R: TTTTTGCTGTGAGTCCCGGAG
OCN (human)	F: AGCAAAGGTGCAGCCTTTGT
	R: GCGCCTGGGTCTCTTCACT
PU.1 (human)	F: GACACGGATCTATACCAACGCC
	R: CCGTGAAGTTGTTCTCGGCGAA
GAPDH (human)	F: CTGGGCTACACTGAGCACC
	R: AAGTGGTCGTTGAGGGCAATG
Mmp25 (mouse)	F: TGGAATGGCTGACTCGCTATG
	R: GCATGACTTTGATTGCATCCTG
P16 (mouse)	F: CGCAGGTTCTTGGTCACTGT
	R: TGTTCACGAAAGCCAGAGCG
P21 (mouse)	F: CCTGGTGATGTCCGACCTG
	R: CCATGAGCGCATCGCAATC
PU.1 (mouse)	F: TTCAGAGCTATACCAACGTCCA
	R: TGATCGCTATGGCTTTCTCCA
Gapdh (mouse)	F: AGCCCAGAACATCATCCCTG
	R: CACCACCTTCTTGATGTCATC

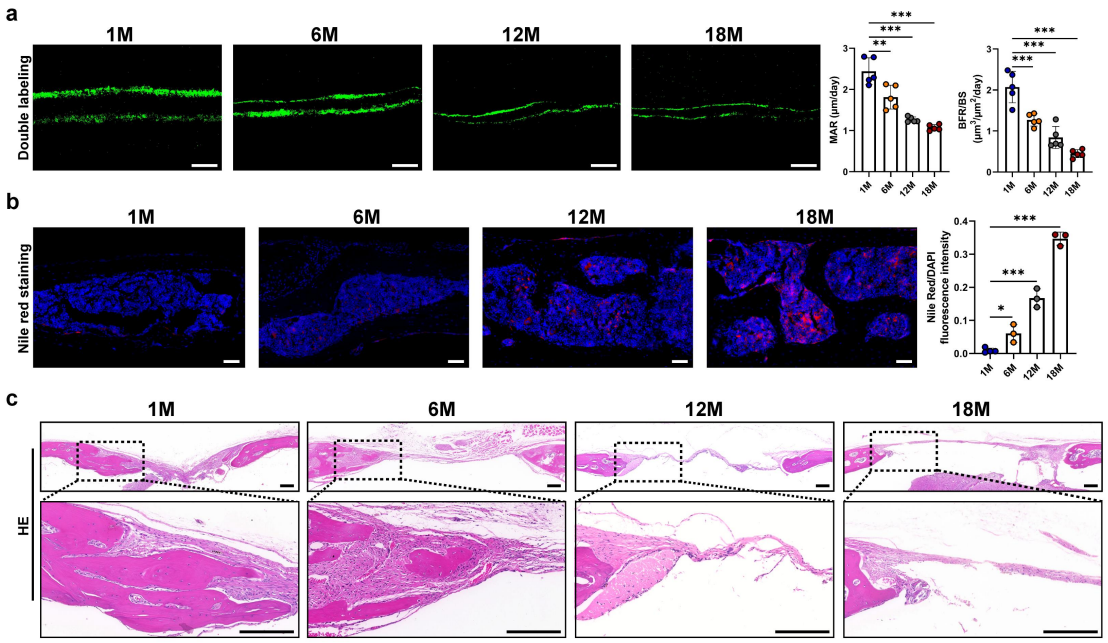

Figure S1 (related to Figure 1). Age-related changes in skull bone formation and marrow adiposity

(a) Representative images (left) of calcein double labeling in parietal bone from 1M, 6M, 12M, and 18M mice, and quantification of MAR and BFR (right). *n* = 5. Scale bar, 20 μm.

(b) Nile red staining of lipids (red) in the skull BM from mice of different ages. Quantification of the Nile red fluorescence intensity is shown on the right. *n* = 3. Scale bar, 50 μm.

(c) Representative H&E staining of calvarial defects 8 weeks after surgery in 1M, 6M, 12M, and 18M mice. Scale bar, 200 μm.

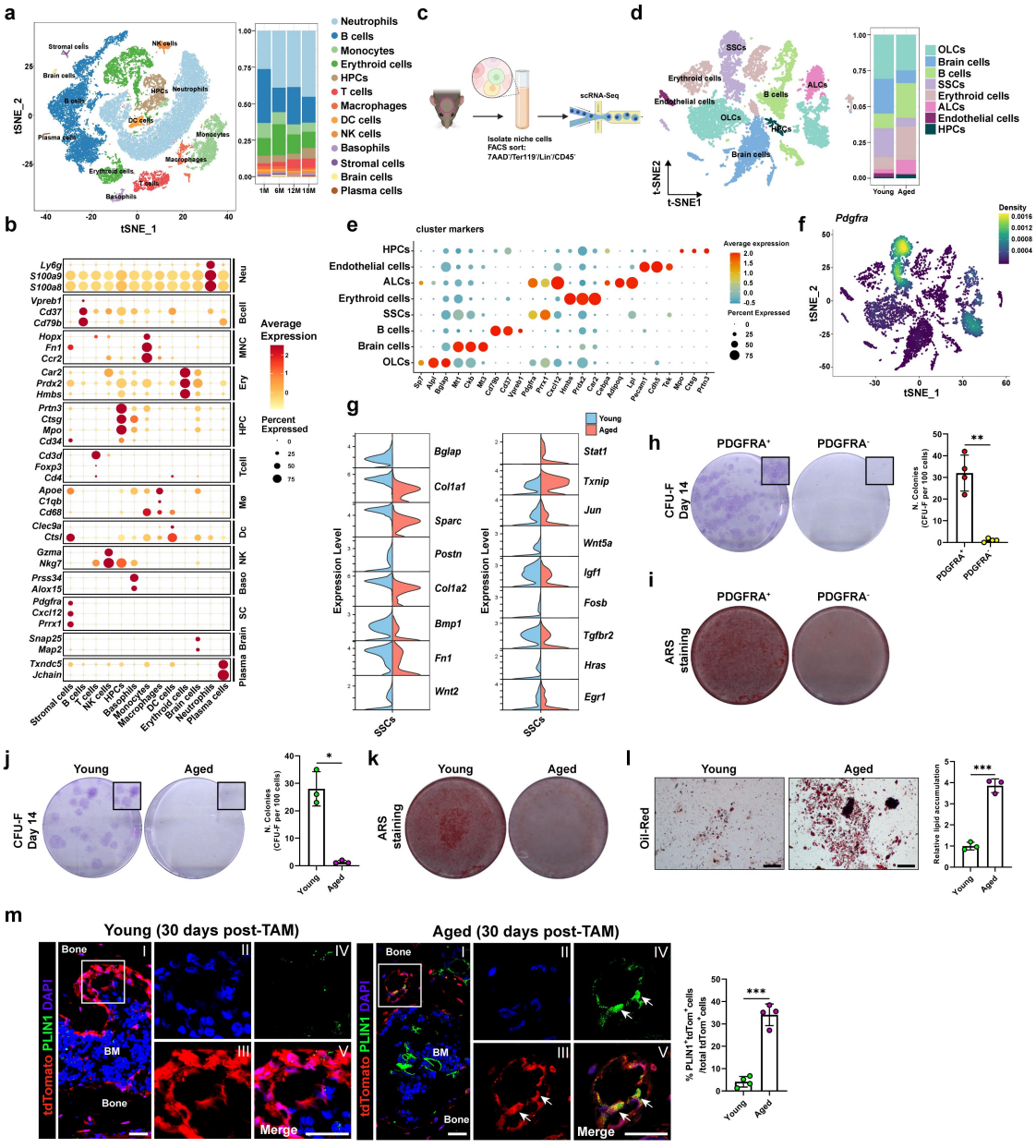

Figure S2 (related to Figure 1). Characterization and age-related changes of PDGFRA$^+$ SSCs

(a) scRNA-seq analysis of skull BM cells from 1M, 6M, 12M, and 18M mice. t-distributed stochastic neighbor embedding (t-SNE) visualization showing distinct cell populations color-coded by cell type (left) and quantification of cell proportions (right). HPCs: hematopoietic progenitor cells.

(b) Gene expression dotplots showing cell-type specific markers in skull BM cells.

(c) Experimental strategy for single-cell transcriptomic analysis of skull BM cells. Created in BioRender.

(d) t-SNE visualization of scRNA-seq data from young (1M) and aged (12M) $7AAD^-/Ter119^-/Lin^-/CD45^-$ cells showing distinct cell populations color-coded by cell type (left) and quantification of cell proportions (right). Cell populations include skeletal stem cells (SSCs), osteogenic lineage cells (OLCs), adipogenic lineage cells (ALCs), HPCs, B cells, brain cells, erythroid cells, and endothelial cells.

(e) Gene expression dotplot showing cluster-defining marker genes across identified cell populations.

(f) t-SNE visualization showing *Pdgfra* expression distribution in cells from young (1M) mice. Color intensity represents expression density of the *Pdgfra* gene across the identified cell populations.

(g) Transcriptional Profiles of Proliferation, Apoptosis, and Osteogenesis in SSCs between Young and Aged Mice.

(h) CFU-F analysis and quantification of $PDGFRA^+$ and $PDGFRA^-$ populations. n = 4.

(i) ARS staining of osteogenic differentiation from $PDGFRA^+$ and $PDGFRA^-$ cells.

(j) CFU-F analysis and quantification of young (1M) and aged (12M) $PDGFRA^+$ SSCs. n = 3.

(k) ARS staining of osteogenic differentiation of young (1M) and aged (12M) PDGFRA^{+} SSCs.

(l) Oil Red O staining and quantification of adipogenic differentiation of young (1M) and aged (12M) PDGFRA^{+} SSCs. *n* = 3. Scale bar, 100 μm.

(m) Immunofluorescence staining of Perilipin 1 (PLIN1) in skull bone sections from young (1M) and aged (12M) *Pdgfra-CreER^{T2}tdTomato* mice at 30 days post-tamoxifen induction. Representative images are shown (left) and quantification of PLIN1^{+} tdTomato^{+} double-positive cells as a percentage of total tdTomato^{+} cells is presented (right). *n* = 4. Scale bar, 25 μm.

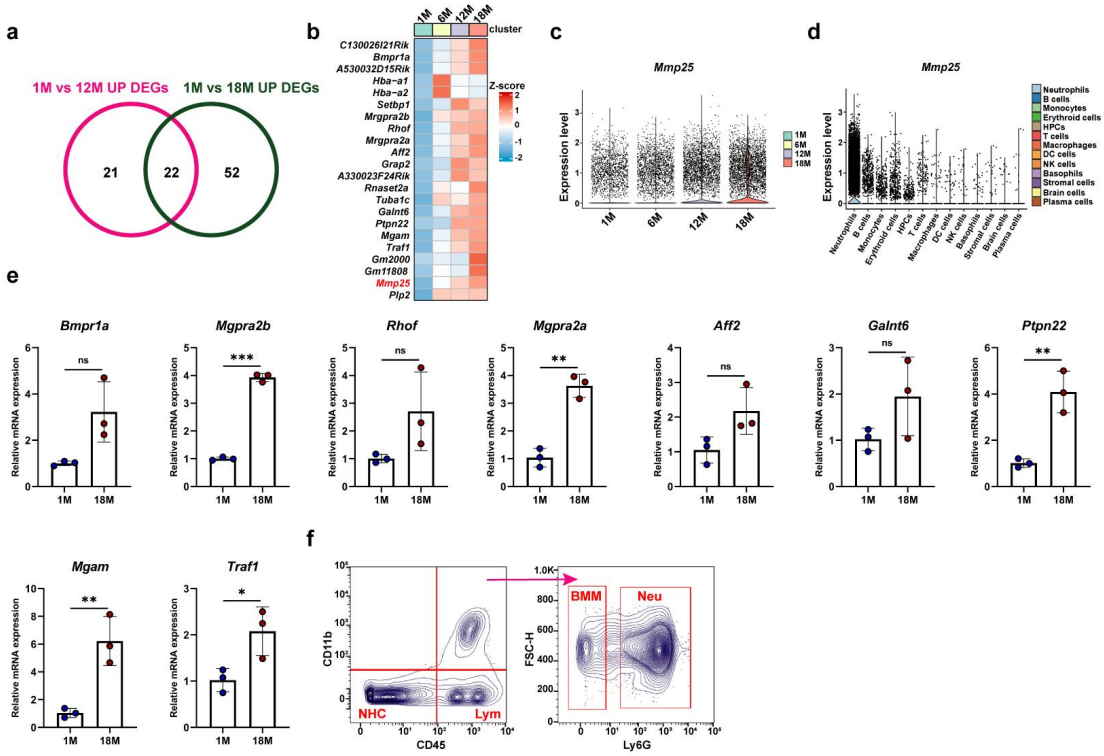

Figure S3 (related to Figure 2). Single-cell transcriptomic analysis identifies neutrophil-derived *Mmp25* as an age-associated inflammatory gene

(a) Venn diagram showing the overlap of upregulated differentially expressed genes (DEGs) in skull BM cells from aged (12M and 18M) mice compared to young (1M) mice, as identified by scRNA-seq analysis. DEGs were identified using criteria of log2FC > 1.3 and adjusted $p < 0.05$ from scRNA-seq analysis.

(b) Heatmap showing expression patterns of 22 overlapping DEGs in skull BM cells from mice of different ages (1M, 6M, 12M, and 18M).

(c-d) Violin plots showing the expression of *Mmp25* in skull BM from mice of different ages (c) and across different cell populations (d).

(e) qPCR validation of DEGs identified in (b). $n = 3$.

(f) Representative flow cytometry plots showing the gating strategy for identifying the NHC, Lym, BMM, and Neu populations.

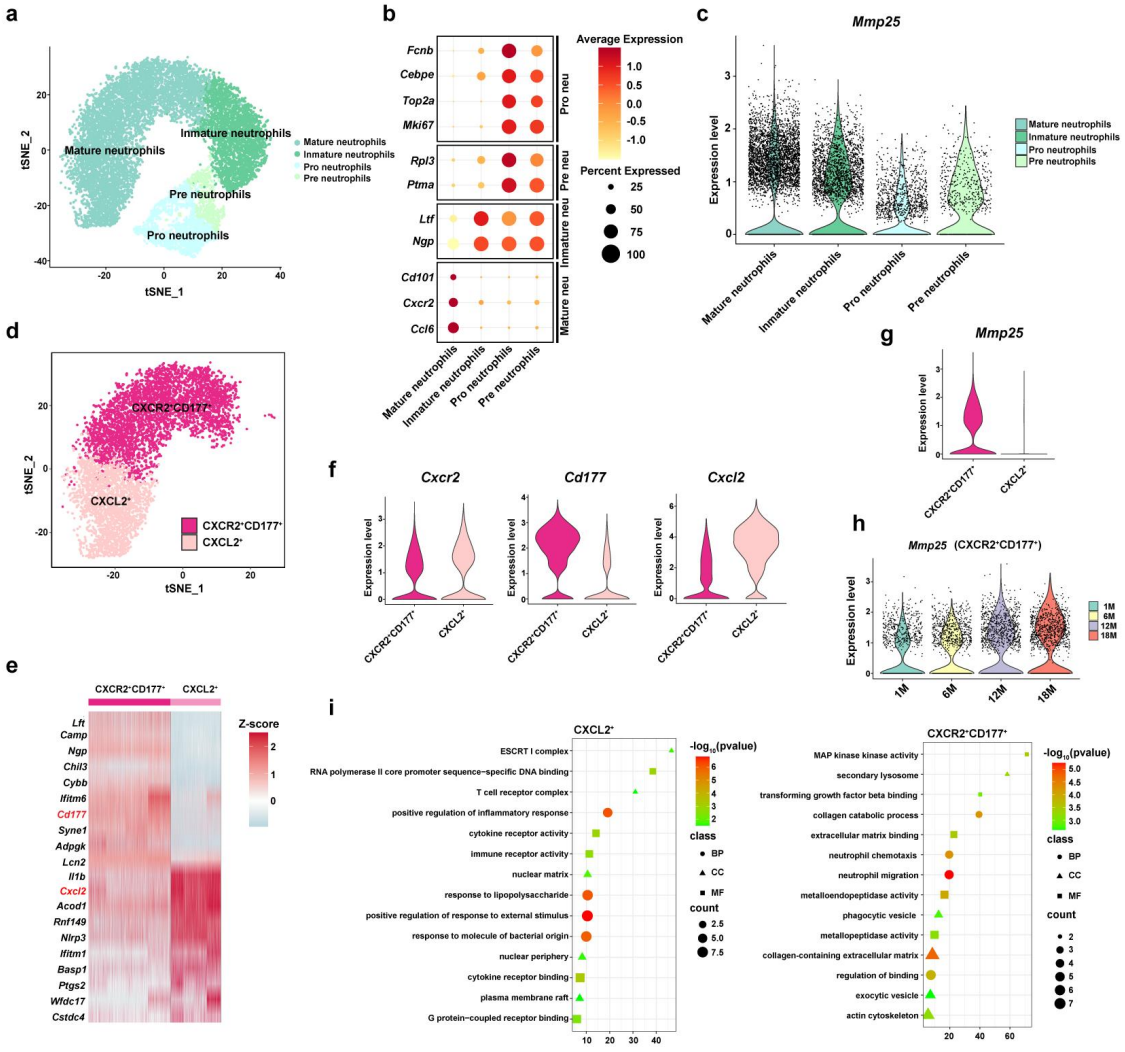

Figure S4 (related to Figure 2). Single-cell analysis identifies an age-accumulating CXCR2^{+}CD177^{+} neutrophil subset with high *Mmp25* expression

(a) t-SNE plot of neutrophil subsets isolated from mice with different ages (1M, 6M, 12M and 18M).

(b) Dotplot analysis of subset-specific marker genes defining neutrophil subsets.

(c) Violin plots showing expression of *Mmp25* across different neutrophil subsets.

(d) t-SNE visualization showing CXCL2^{+} and CXCR2^{+}CD177^{+} mature neutrophil

subsets.

(e) Gene expression heatmap of top 10 genes expressed in mature neutrophil subsets.

(f) Violin plots showing the expression of *Cxcr2*, *Cd177*, and *Cxcl2* in $CXCL2^+$ and $CXCR2^+CD177^+$ mature neutrophil subsets.

(g) Violin plots showing enriched *Mmp25* expression in $CXCR2^+CD177^+$ versus $CXCL2^+$ neutrophil subsets.

(h) Violin plots showing increased expression of *Mmp25* with age in $CXCR2^+CD177^+$ neutrophil subsets.

(i) Gene Ontology enrichment analysis revealed distinct functional signatures of $CXCL2^+$ (left) and $CXCR2^+CD177^+$ (right) neutrophil subsets.

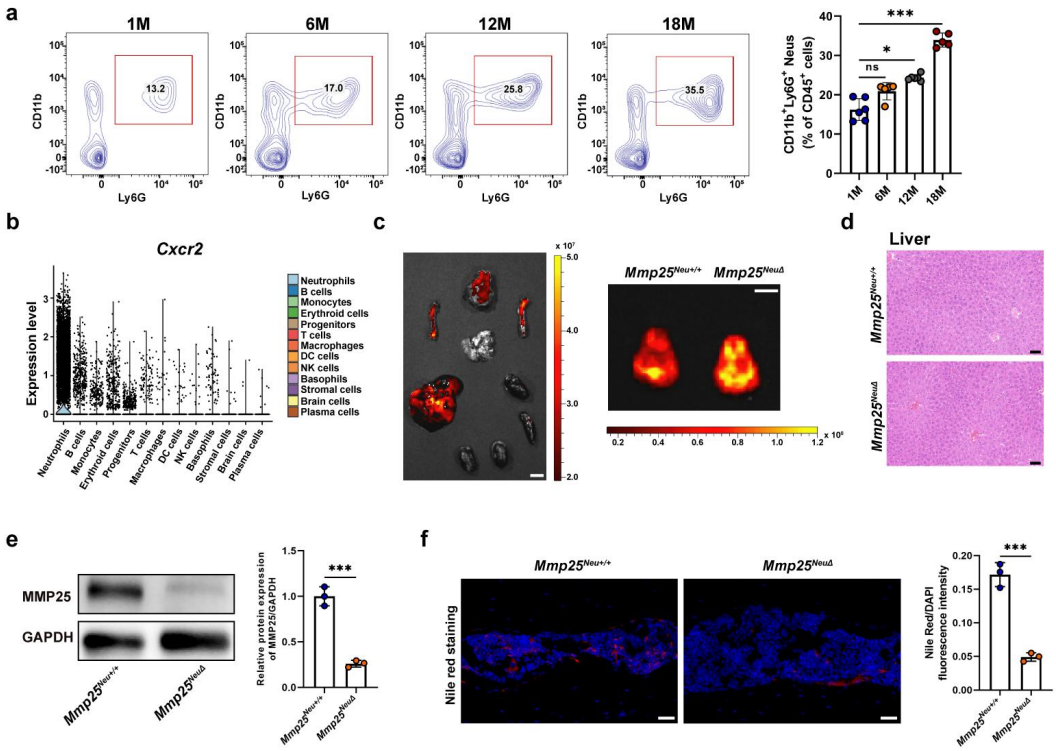

Figure S5 (related to Figure 2). Validation of the AAV9-*Cxcr2* system and age-associated accumulation of MMP25-expressing neutrophils in skull BM

(a) Representative flow cytometry plots showing age-dependent increases in $CD11b^{+}Ly6G^{+}$ neutrophils from skull BM of 1M, 6M, 12M, and 18M groups (left) and quantification of neutrophil frequency (right). *n* = 6 mice in the 1M and 12M groups; *n* = 5 mice in the 6M and 18M groups.

(b) Violin plots showing the expression of *Cxcr2* across different cell populations in skull BM.

(c) *In vivo* fluorescence imaging showing the biodistribution of AAV9-*Cxcr2*-eGFP in mice following systemic administration. Fluorescent signals were predominantly detected in skeletal tissues, especially in craniofacial bones. Scale bars, 1 cm.

(d) Representative H&E staining of liver sections from *Mmp25*$^{Neu+/+}$ and *Mmp25*^{NeuΔ} mice. Scale bars, 50 μm.

(e) Western blot analysis showing MMP25 protein levels in neutrophils from *Mmp25*$^{Neu+/+}$ and *Mmp25*^{NeuΔ} mice. $n = 3$.

(f) Nile red staining and quantification of lipids in skull BM from *Mmp25*$^{Neu+/+}$ and *Mmp25*^{NeuΔ} mice. $n = 3$. Scale bar, 50 μm.

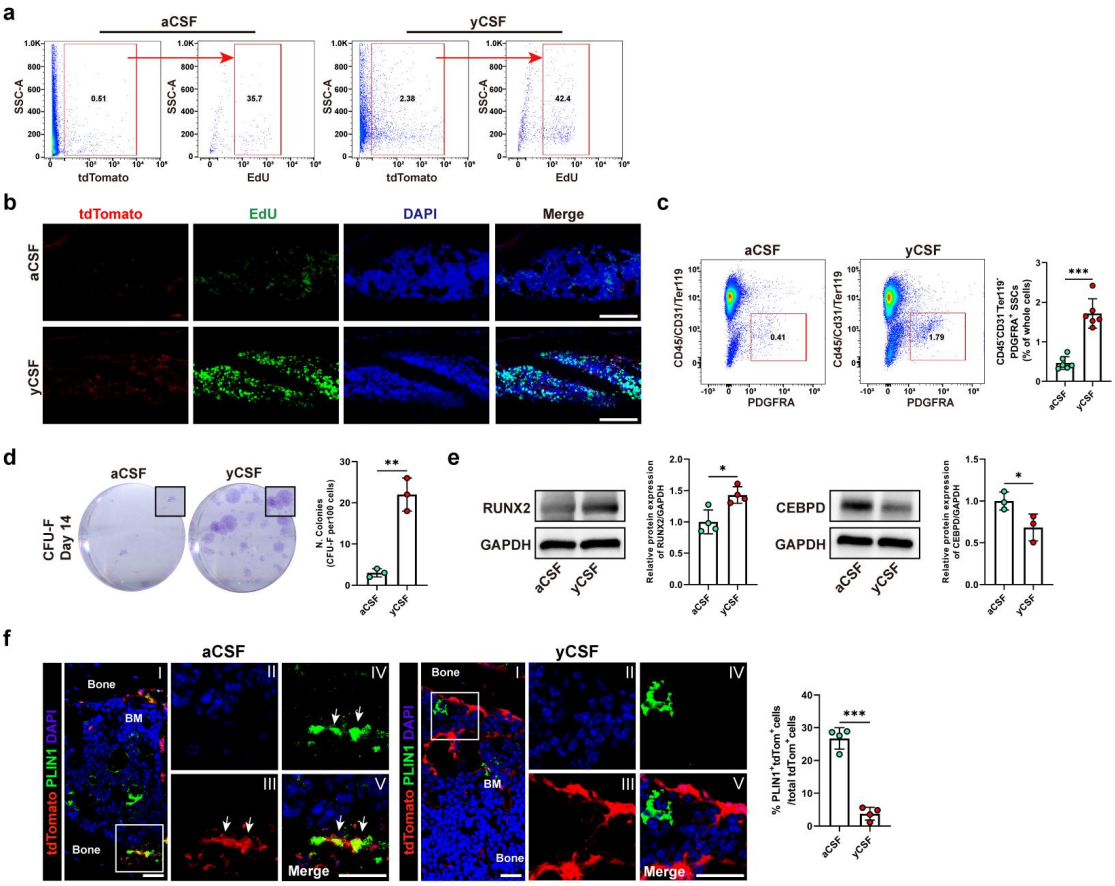

Figure S6 (related to Figure 4). yCSF promotes proliferation and osteogenic differentiation of PDGFRA$^+$ SSCs

(a) Representative flow cytometry plots showing tdTomato$^+$ and EdU$^+$ cells in *Pdgfra-CreER^{T2}tdTomato* mice 72 hours after aCSF or yCSF treatment.

(b) Representative immunofluorescence images showing EdU$^+$ cells (green) and tdTomato$^+$ cells (red) in the skull BM from aged (12M) *Pdgfra-CreER^{T2}tdTomato* mice 72 h after aCSF or yCSF treatment. Scale bar, 100 μm.

(c) Flow cytometry analysis and quantification of PDGFRA$^+$ SSCs in skull BM from aged (12M) mice 7 days after aCSF or yCSF treatment. $n = 6$.

(d) CFU-F analysis and quantification of PDGFRA$^+$ SSCs isolated from aged (12M)

mice 7 days after aCSF or yCSF treatment. $n = 3$.

(e) Western blot analysis and quantification of RUNX2 and CEBPD expression in PDGFRA$^+$ SSCs isolated from aged (12M) mice 7 days after aCSF or yCSF treatment. $n = 4$ for RUNX2, and $n = 3$ for CEBPD.

(f) Representative immunofluorescence images of skull BM sections from aCSF- or yCSF-treated aged (12M) *Pdgfra-CreER^{T2}tdTomato* mice showing PLIN1 expression (green) in tdTomato$^+$ cells (red). quantification of PLIN1$^+$tdTomato$^+$ double-positive cells as a percentage of total tdTomato$^+$ cells is presented (right). $n = 4$. Scale bar, 25 μm.

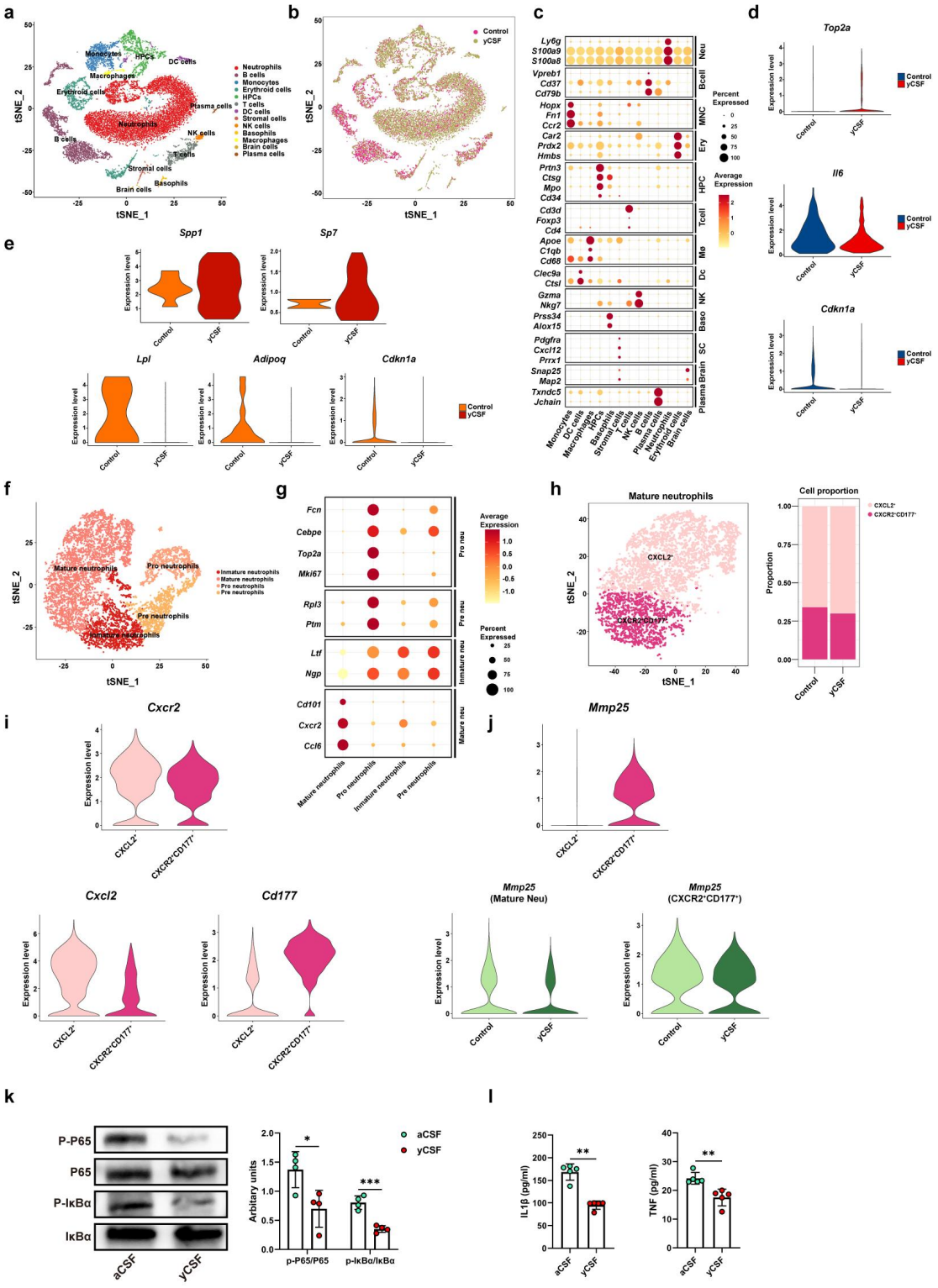

Figure S7 (related to Figure 4). Single-cell analysis reveals yCSF induced remodeling of aged BM

(a-b) t-SNE plot of skull BM cells from control and yCSF-treated mice.

(c) Gene expression dotplots showing cell-type specific markers in skull BM cells.

(d) Violin plots showing the expression of *Top2a*, *Il6*, and *Cdkn1a* in BM cells from control and yCSF-treated mice.

(e) Violin plots showing the expression of *Spp1*, *Sp7*, *Lpl*, *Adipoq*, and *Cdkn1a* in stromal cells from control and yCSF-treated mice.

(f) t-SNE plot of neutrophils and mature neutrophil subsets.

(g) Dotplot analysis of subset-specific marker genes defining neutrophil subsets.

(h) Proportion of $CXCL2^+$ and $CXCR2^+CD177^+$ cells in mature neutrophils from control and yCSF-treated mice.

(i) Violin plots showing the expression of *Cxcr2*, *Cxcl2*, and *Cd177* in $CXCL2^+$ and $CXCR2^+CD177^+$ mature neutrophil subsets.

(j) Violin plots showing *Mmp25* expression in mature neutrophils and the $CXCR2^+CD177^+$ population in control and yCSF-treated mice.

(k) Western blot analysis of p-P65, P65, p-IκBα, and IκBα protein levels in neutrophils isolated from aged (12M) mice 7 days after aCSF or yCSF treatment. Quantification of p-P65/P65 and p-IκBα/IκBα ratios is shown (right). $n = 4$.

(l) ELISA quantification of IL1β and TNF in skull BM supernatant from aCSF and yCSF-treated mice. $n = 5$.

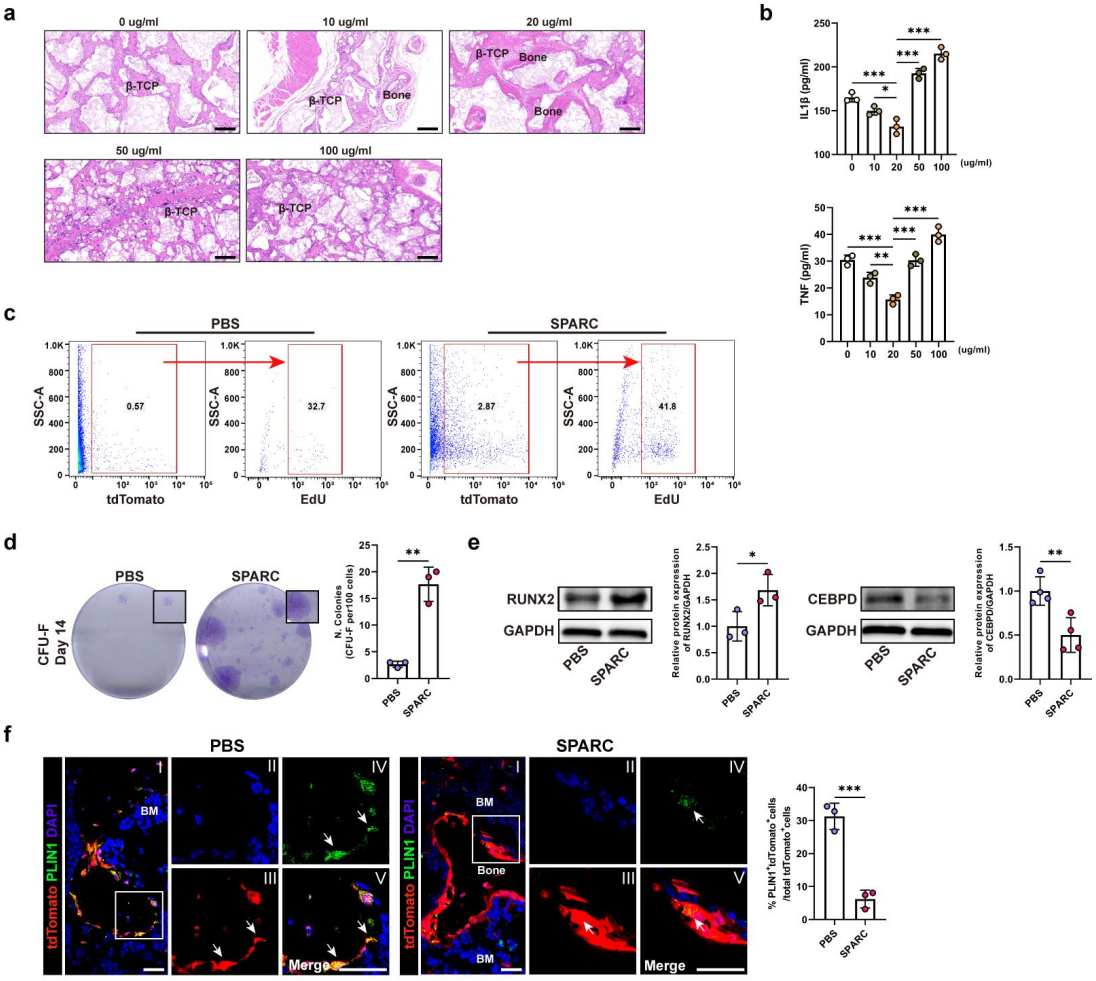

Figure S8 (related to Figure 5). SPARC enhances the function of aged PDGFRA$^+$ cells

(a) H&E staining of ectopic bone formation by PDGFRA$^+$ SSCs isolated from aged (12M) mice treated with different concentrations of SPARC (0, 10, 20, 50, 100 μg/mL) for 7 days, followed by subcutaneous transplantation with β-TCP scaffold for 4 weeks. Scale bar, 100 μm. $n = 3$.

(b) ELISA quantification of IL1β and TNF in skull BM supernatant from aged (12M) mice treated with different concentrations of SPARC (0, 10, 20, 50, 100 μg/mL) for 7 d. $n = 3$.

(c) Representative flow cytometry plots showing tdTomato$^+$ and EdU$^+$ cells in *Pdgfra-CreER^{T2}tdTomato* mice 72 hours after PBS or SPARC treatment.

(d) CFU-F analysis and quantification of PDGFRA$^+$ SSCs isolated from aged (12M) mice after 7-day SPARC treatment. $n = 3$.

(e) Western blot analysis and quantification of RUNX2 (e) and CEBPD (f) in PDGFRA$^+$ SSCs following 7-day SPARC treatment. $n = 3$ for RUNX2, and $n = 4$ for CEBPD.

(f) Representative immunofluorescence images of skull BM sections from PBS- or SPARC-treated aged (12M) *Pdgfra-CreER^{T2}tdTomato* mice showing PLIN1 expression (green) in tdTomato$^+$ cells (red). quantification of PLIN1$^+$tdTomato$^+$ double-positive cells as a percentage of total tdTomato$^+$ cells is presented (right). $n = 3$. Scale bar, 25 μm.

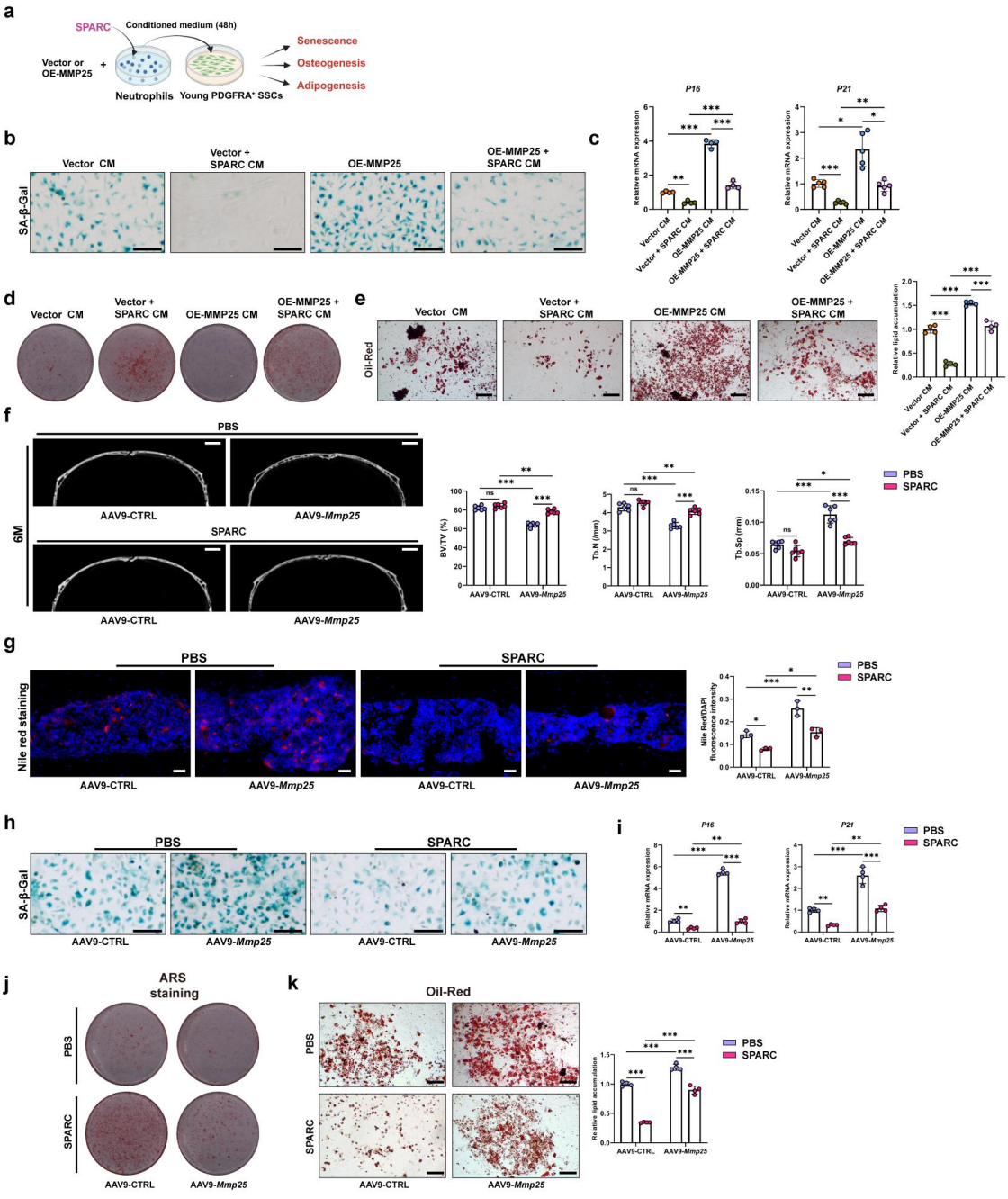

Figure S9 (related to Figure 5). SPARC enhances the function of aged PDGFRA^{+} cells

(a) Schematic diagram showing the experimental design, where CM was collected from neutrophils isolated from 12-month-old mice, transfected with the vector or OE-MMP25, with or without SPARC treatment for 48 hours, followed by the analysis

of senescence, osteogenesis, and adipogenesis in young (1M) PDGFRA$^+$ SSCs.

(b) Representative SA-β-Gal staining of senescent cells in young (1M) PDGFRA$^+$ SSCs treated with CM from neutrophils transfected with vector or OE-MMP25, with or without SPARC treatment. n = 3. Scale bar, 100 μm.

(c) qPCR analysis of P16 (n = 4) and P21 (n = 5) mRNA expression in PDGFRA$^+$ SSCs cultured with different CM.

(d) ARS staining of osteogenic differentiation in young (1M) PDGFRA$^+$ SSCs treated with CM from the indicated neutrophil groups.

(e) Oil Red O staining and quantification of adipogenic differentiation in young (1M) PDGFRA$^+$ SSCs treated with CM from the indicated neutrophil groups. n = 4. Scale bar, 100 μm.

(f) Representative μCT images (left) and quantification (right) of skull from 6M group mice following 2-month treatment with AAV9-CTRL or AAV9-*Mmp25* with or without SPARC treatment. n = 6. Scale bar, 1 mm.

(g) Representative images showing lipid accumulation by Nile red staining in skull BM from aged (12M) mice following 2-months of AAV9-CTRL or AAV9-*Mmp25* treatment, with or without SPARC. Quantification of Nile red/DAPI fluorescence intensity is shown on the right. n = 3. Scale bar, 50 μm.

(h) SA-β-Gal staining of senescent cells in PDGFRA$^+$ SSCs isolated from skull BM of aged mice treated with AAV9-CTRL or AAV9-*Mmp25* with or without SPARC. n = 3. Scale bar, 100 μm.

(i) qPCR analysis of *P16* and *P21* mRNA expression in PDGFRA$^+$ SSCs isolated

from skull BM of aged mice treated with AAV9-CTRL or AAV9-*Mmp25* with or without SPARC. $n = 4$.

(j) ARS staining of osteogenic differentiation in PDGFRA$^+$ SSCs isolated from skull BM of aged mice treated with AAV9-CTRL or AAV9-*Mmp25* with or without SPARC.

(k) Oil-red-O staining of adipogenic differentiation in PDGFRA$^+$ SSCs isolated from skull BM of aged mice treated with AAV9-CTRL or AAV9-*Mmp25* with or without SPARC. $n = 3$. Scale bar, 100 μm.

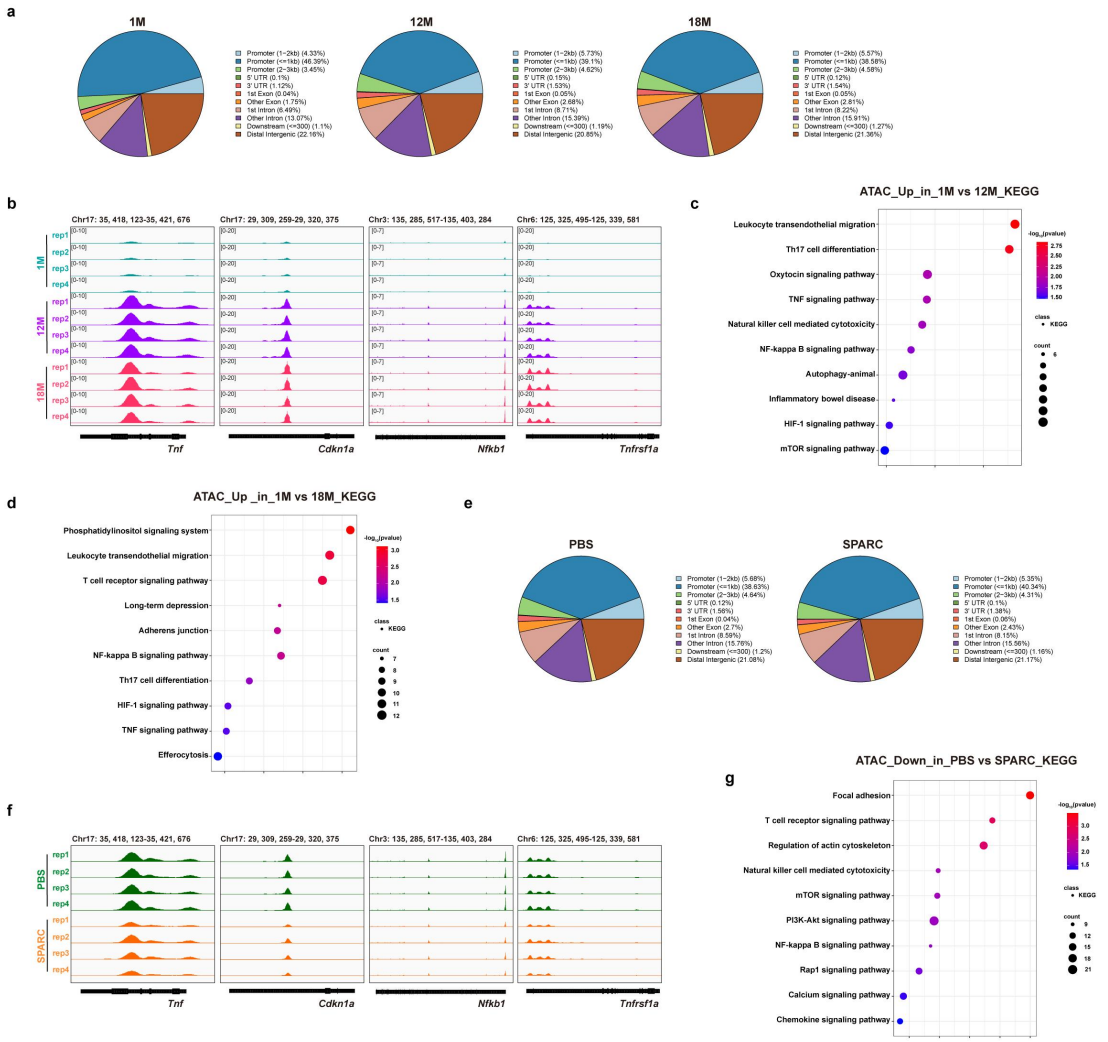

Figure S10 (related to Figure 6). Chromatin accessibility changes in skull neutrophils during aging and following SPARC intervention

(a) Pie chart showing the distribution of ATAC-seq peaks identified in neutrophils from 1-, 12-, and 18-month-old mice.

(b) Representative ATAC-seq tracks of the *Tnf*, *Cdkn1a*, *Nfkb1*, and *Tnfrsf1a* loci in skull neutrophils of 1-, 12-, and 18-month-old mice.

(c) KEGG pathway analysis of ATAC-seq peaks that were increased in 12-month-old mice compared to 1-month-old mice.

(d) KEGG pathway analysis of ATAC-seq peaks that were increased in 18-month-old mice compared to 1-month-old mice.

(e) Pie chart showing the distribution of ATAC-seq peaks identified in neutrophils of aged mice treated with PBS or SPARC for 7 days.

(f) Representative ATAC-seq tracks of the *Tnf*, *Cdkn1a*, *Nfkb1*, and *Tnfrsf1a* loci in skull neutrophils of aged mice treated with PBS or SPARC for 7 days.

(g) KEGG pathway analysis of ATAC-seq peaks that were decreased in SPARC-treated mice compared to PBS-treated mice.

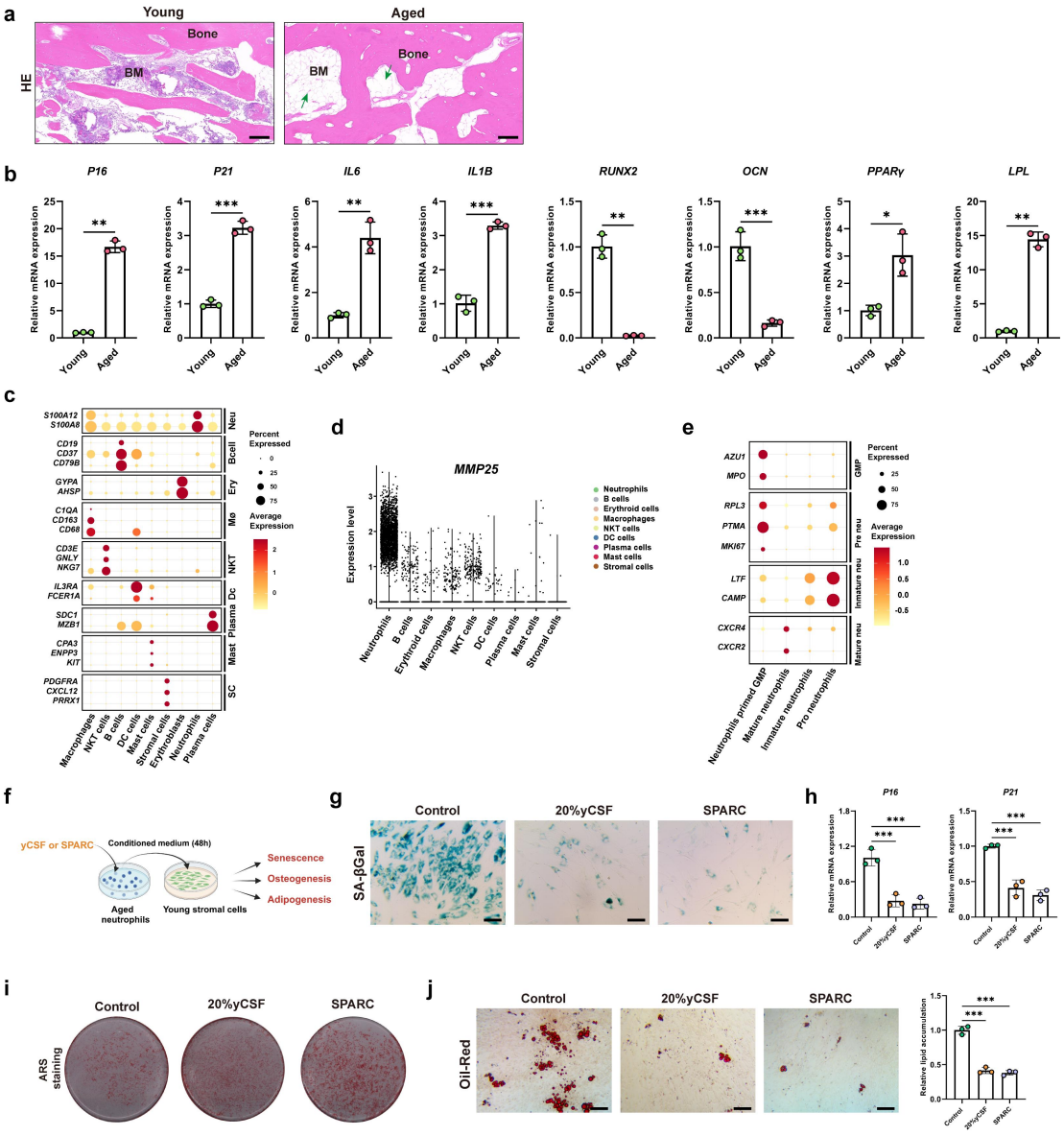

Figure S11 (related to Figure 7). SPARC and yCSF revitalize aged human BM

(a) Representative H&E staining of young and aged human skull sections. Green arrows indicate adipose vacuoles in the BM. Scale bar, 200 μm.

(b) qPCR analysis of senescence-associated (*P16*, *P21*), inflammatory (*IL6*, *IL1B*), osteogenic (*RUNX2*, *OCN*), and adipogenic (*PPARγ*, *LPL*) genes in BM cells from young and aged individuals. $n = 3$.

(c) Gene expression dotplots showing cell-type specific markers in human skull BM

cells.

(d) Violin plots showing the expression of *MMP25* across different cell populations.

(e) Dotplot analysis of subset-specific marker genes defining human neutrophil subsets.

(f) Schematic diagram showing the CM collected from aged neutrophils treated with yCSF or SPARC, followed by functional analysis of BM stromal cells isolated from young individuals. Created in BioRender.

(g) Representative SA-β-Gal staining of senescent cells in young stromal cells treated with CM from aged neutrophils with indicated treatments. $n = 3$. Scale bar, 100 μm.

(h) qPCR analysis of *P16* and *P21* mRNA expression in young stromal cells treated with different CM. $n = 3$.

(i) ARS staining of osteogenic differentiation in young stromal cells treated with CM from aged neutrophils with indicated treatments.

(j) Oil Red O staining and quantification of adipogenic differentiation in young stromal cells treated with CM from aged neutrophils with indicated treatments. $n = 3$.